Universidad de La Laguna

Máster Universitario en Energías Renovables

Spectral Characterization of Solar Cells

Trabajo Fin de Máster

La Laguna, 4 de Septiembre 2018

Autora: Silvia Cal Ramírez
Tutor: Cecilio Hernández Rodríguez

Spectral Characterization of Solar Cells

In this work, experimental measurements of Spectral Response (SR), External Quantum Efficiency (EQE), and Internal Quantum Efficiency (IQE) of different mono-crystalline and multi-crystalline silicon solar cells have been carried out. Additionally, the spectral characterization of a mono-crystal silicon reference cell in the range (UV-VIS-NIR) and a photodiode of GaAsP in the UV-VIS range were verified. The Intensity - Voltage (IV) curves of the solar cells studied were also experimentally determined. Measurements were carried out at the photovoltaic laboratory of the Technological and Renewable Energies Institute (ITER), known as SiCell Lab, and at the Optics Laboratory of University of La Laguna (ULL). From the results obtained we can confirm the future study of new materials, as well as contributing in the development of a laboratory at University of La Laguna which will allow experimental practices in Solar Energy for students of the Master in Renewable Energies.

Silvia Cal Ramírez [(1)], [(2)]

(1) Universidad de La Laguna, Departamento de Física, Apartado 456, 38200 La Laguna. Santa Cruz de Tenerife – España.
(2) Instituto Tecnológico y de Energías Renovables, S.A. (ITER, S.A.). Polígono Industrial de Granadilla, s/n 38600 - Granadilla de Abona. Santa Cruz de Tenerife – España.

C O N T E N T S

1. Introduction

Solar cells are devices that convert solar light into electricity by means of a physical phenomenon known as photovoltaic effect (Becquerel, 1839). The solar cell has the capacity to absorb light, delivering part of the energy of the absorbed photons to the charge carriers (electrons and holes). A semiconductor diode separates and collects these charge carriers, conducting the generated electrical current in a specific direction. Thus, a solar cell is in essence a semiconductor diode that has been designed to efficiently absorb and convert the energy of sunlight into electrical energy [1].

Sunlight is incident from the top of the solar cell. A metallic grid forms one of the electrical contacts of the diode, allowing light to fall between the grid lines of the semiconductor to be absorbed and converted into electrical energy. An antireflective layer between the grid lines is used to avoid possible reflections in the surface, therefore increasing the amount of light transmitted to the semiconductor. The semiconductor diode, formed when an n-type and a p-type semiconductor are brought together to create a metallurgical junction, is a decisive element in the overall device. The physical mechanism of operation of the junction will be explained in more detail in the next section. This p-n junction is typically achieved through diffusion or implantation of specific impurities, known as dopants, or via a deposition process. The other electrical contact is on the back surface of the solar cell, formed by a metallic layer [2].

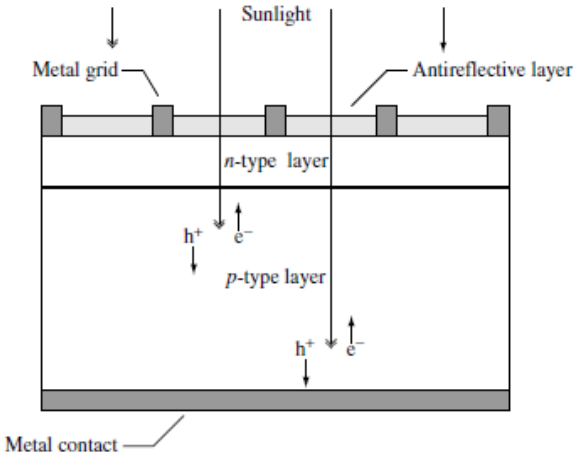

Figure 1. Schematic of a conventional solar cell. Creation of electron-hole pairs, e^- and h^+, respectively, is depicted [2].

1.1. The Potential Barrier: p-n homojunction

To comprehend the physical mechanism of a solar cell it is important to understand the p-n junction. The generation of electrons and holes by light is the central process in the overall photovoltaic effect, but it does not itself produce current. An in-built voltage across the junction is needed to get the charge carriers to generate electric current. Otherwise, the light-generated electron-hole pairs would eventually lose their gained energy by thermal processes, causing the electron to fall from the conduction band to the valence band [3].

There are several ways to form a potential barrier in a solar cell, being the most common the p-n junction. Conceptually, a p-n junction is formed when a layer of doped silicon is brought in contact with an oppositely doped base layer of silicon [3]. Usually, one layer of silicon is doped with boron (a p-type dopant) and the other layer with phosphorus (an n-type dopant). The n-type semiconductor has large concentration of free electrons that is compensated by positive ions (phosphorus atoms). On the contrary, in the p-type semiconductor holes are the majority carriers and their positive charge is compensated by negative ions (boron atoms) [4].

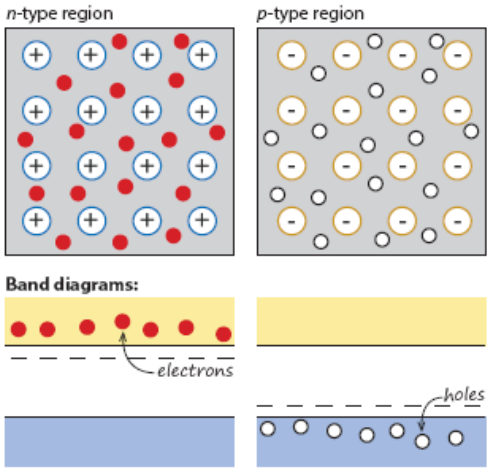

Figure 2. Schematic representation of an isolated n-type and p-type semiconductor and corresponding band diagrams [4].

When a p-type and an n-type semiconductor are brought together, the large concentration of mobile electrons on the n-type region versus the p-type region regions causes a diffusion current of electrons from the n-type material into the p-type material. Similarly, the difference in holes concentration on the p-type side causes the holes to diffuse into the n-type side [4].

Due to this diffusion process, the region close to the interface between the n and p regions becomes almost completely depleted of mobile charge carriers. Electrons leave behind positively charged phosphorus ions and holes leave negatively charged boron ions. This phenomenon gives rise to the so-called space-charge region or depleted region, created by the charge of the ionized phosphorus (donor) and boron (acceptor) atoms that is not compensated by the mobile charges [4,5].

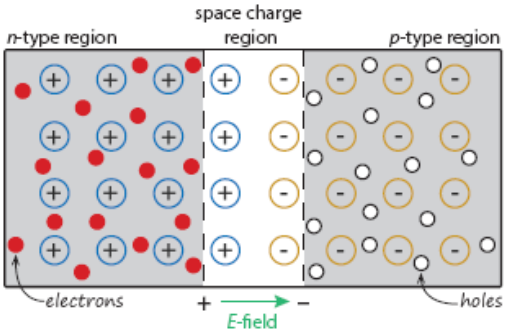

Figure 3. Formation of a space-charge region, where n-type and p-type semiconductor are brought together to form a junction [4].

These fixed ions results in the formation of an electric field at the junction which forces the charge carriers to move in the opposite direction than the concentration gradient. The diffusion current continues to flow until eventually reaching equilibrium where the concentration gradient and the internal electrical field compensate each other. Thus, a difference in electrostatic potential is developed across the space-charge region under equilibrium conditions and it is denoted as the built-in voltage, V_{bi}, which is the potential difference at the edges of the space-charge region [4].

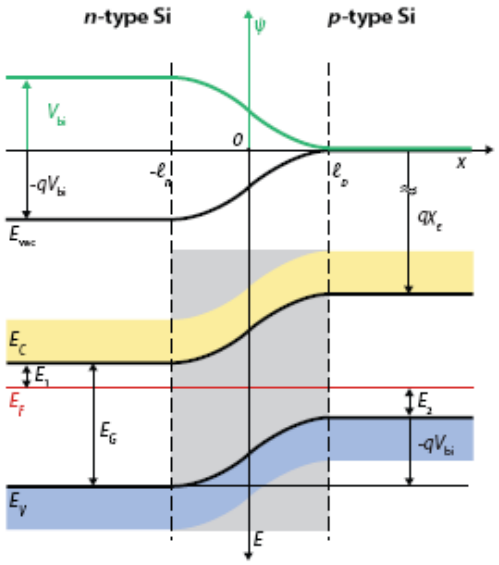

Figure 4. Energy-band diagram of the p-n junction under equilibrium. The electrostatic potential profile (green curve) is also presented [4].

The p-n junction does not allow the formation of current due to the depletion region. However, if a voltage higher than the existing barrier in this area is applied the device can produce current. Direct polarization of a p-n junction consists in applying a positive tension to the p-type region and negative to the n-type region. This way, the potential barrier is overcome and there is movement of the charge carriers. Incident light can create additional electron-hole pairs, and the intrinsic field generated by the p-n junction (0.7 V for Silicon) separates them, thereby preventing recombination and producing photo-generated electric current. The most important parameters of a semiconductor material in solar cells are the energy of the gap, the number of free carriers for conduction and the generation or recombination of charge carriers in response to sunlight [6].

1.2. Efficiency losses

The incident photons in a solar cell can be absorbed, transmitted or reflected. Absorbed photons whose energy is greater than the gap promote an electron to the conduction band, generating an electron-hole pair. If the generation takes place at a distance from the junction lower than the diffusion length (length that the carriers travel before recombining), the electric field existing at the p-n junction can separate these charge carriers, moving the electrons to the n-type region and the holes to the p-type region. If both regions are connected to an external circuit, an electric current is

generated. Thus, in a solar cell the absorption must be maximum and the recombination and reflection as low as possible [6].

The main losses in a standard solar cell are depicted in Figure 5. The most significant power-loss mechanism in single-bangap cells are the inability to absorb photons having lower energy than the bandgap (1 in Fig. 5) and thermalization of highly energetic photons, whereby the photo-excited pair quickly loses the extra energy exceeding the bandgap (2 in Fig. 5). A low-energy red photon is just as effective as a much higher energetic blue photon. These two effects alone can account for the loss of about 50% of the incident radiant energy in the solar cell conversion to electricity [7].

Another important loss mechanism is process 5, recombination of the generated electron–hole pairs. By removing all unnecessary defects and employing material with high lifetimes for the generated charge carriers, this effect can be kept to a minimum [8].

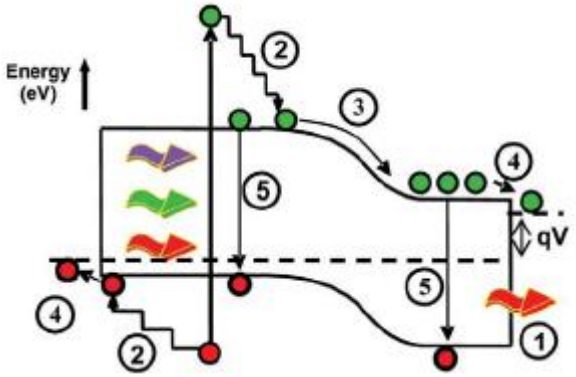

Figure 5. Loss processes in a standard solar cell: (1) non-absorption of below-bandgap photons (2) lattice thermalization loss; (3) and (4) junction and contact voltage losses; (5) recombination loss (radiative recombination is unavoidable) [7].

The recombination rate is a critical parameter in solar cells and is related to the excess of minority carriers. In the process of recombination, an electron falls from the conduction band to the valence band, thereby eliminating a valence-band hole [6].

There are several recombination mechanisms important to the operation of solar cells being the most significant the recombination through traps (defects) in the forbidden gap, known as Shockley-Read-Hall recombination. Due to this mechanism, defects in the material give rise to recombination centers at localized energy levels within the gap. The recombination occurs through defects present in the material and is carried out in two steps. First, an electron (or hole) is trapped in an energetic state located in the forbidden region introduced by the defects. Then, if a hole (or electron) moves to the same energy state before being re-emitted to the conduction band, it recombines [6].

Other less important recombination mechanisms are radiative recombination (band to band), Auger recombination and surface recombination. This last mechanism appears on the surface of the semiconductor as there is a break in the continuity of the crystal lattice with numerous unsaturated bonds. This effect is usually reduced by using a passivation layer [6].

1.3. Source Spectrum

All electromagnetic radiation, including sunlight, is composed of particles called photons, which carry specific amounts of energy determined by the spectral properties of their source. The amount of energy contained in a photon depends on its color, and each color is associated with a specific value of wavelength, λ, or frequency, *f*, of the corresponding radiation [9]. The photon energy, *E*, is given by the Planck-Einstein relation:

$$E = hf = hc\lambda^{-1} \tag{1}$$

Where *h* is the Planck's constant and *c* is the speed of light. Only photons with sufficient energy to create an electron-hole pair (or exciton), that is, those with energy greater than the semiconductor band gap, E_G, will contribute to the energy conversion process [9]. Thus, the spectral nature of sunlight is an important consideration in the design of efficient solar cells.

The incident solar radiation on the surface of the earth suffers a great atmospheric impact. Phenomena such as absorption and scattering cause changes in the spectral content of solar radiation. Local changes in the composition of the atmosphere, for instance water vapor, aerosols and dust are also added, which affect the power density directionality of the radiation, since they absorb the incident photons. It is considered that the absorption is of the order of 16-24%. Therefore, the energy that reaches the surface has two components, direct and diffuse radiation [10, 11].

The critical parameters when evaluating solar radiation are the followings [6]:

- Spectral content of incident light.
- Power density of solar radiation, also known as Irradiance.
- The angle of incidence.

The efficiency of solar cells is sensitive to variations in irradiance and spectral nature of sunlight. For this reason, it is necessary to define a standard spectrum in order to make comparisons of the behavior of solar cells [6].

The standard spectrum for the surface of the earth is called AM1.5G [12], used for comparing solar cell performance and normalized to a total power density of 1 kW/m² [2]. The term AM (Air Mass) makes reference to the mass of air that radiation passes through in the atmosphere. Thereby, the Air Mass is a measure of how absorption in the atmosphere affects the spectral content and intensity of solar radiation reaching the Earth's surface, given by [6]:

$$Air\ Mass = \frac{1}{\cos\theta} \tag{2}$$

Where θ is the angle of incidence.

The letter G (Global) indicates that both direct and diffuse light are considered. Other common spectrums are [6]:

- AM0: perpendicular incidence of light in outer space. Used to predict the behavior of solar cells in space.
- AM1.5D: angle with respect to the zenith of 48.19º, same as for AM1.5G but only direct radiation is taken into account.

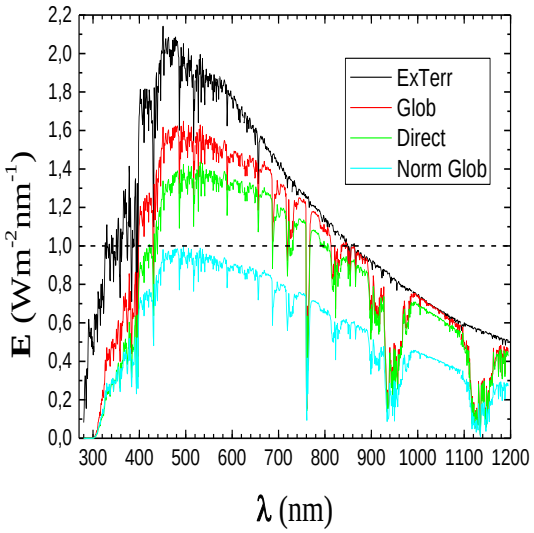

Figure 6. The ASTM G173 spectra represent terrestrial solar spectral irradiance on a surface of specified orientation with an absolute air mass of 1.5 (solar zenith angle 48.19°) (Prepared by the author on the basis of data supplied by [12]).

1.4. Solar cells classification

Photovoltaic solar energy is an alternative for the production of electrical energy that began to develop in the seventies, with efficiencies of 3-5%. Its evolution in the last decades and the improvements introduced are evident, with solar cells reaching efficiencies higher than 27% [6].

Solar cells' classification is generally divided in three generations based on its basic material and the maturity of commercial level [13].

The first generation devices emerge from the technological advances of the microelectronics industry. They are based on single-junction crystalline silicon, which currently remains the most common material for PV devices, being the lead in the commercial market [14]. They demonstrate a performance of about 15-20% and present a high stability [15]. Nevertheless, manufacturing techniques to obtain high efficiency solar cells are expensive and devices need to be several hundred microns thick in order to empower light absorption, representing a significant raw material cost [16].

As a push for cheaper PV devices is sought, second generation devices emerge as an alternative, which benefit from thin-film technology. They are based on amorphous silicon, CIGS and CdTe, where the typical performance is 10-15% [15]. Since these materials have good light absorption, less material is required, resulting in an immediate cost saving. In addition to this, process techniques are less complex and, therefore, it has been possible to reduce production costs compared to the first generation. Additionally, in some instances, as some of the materials can be processed at low temperatures, the possibility of creating devices based on a flexible plastic substrate is offered [16].

However, the production of second generation solar cells still includes vacuum processes and high temperature treatments with the consequent associated energy requirement. Further, the second

generation solar cells are based on scarce elements and this is a limiting factor in the price [15]. Another additional drawback is the poorer material quality that characterizes these devices, which results in the loss of light-generated electrons to defects in the structure with the corresponding reduction in efficiency [16].

Third generation devices encompass a vast range of technologies, aimed at decreasing production costs by significantly increasing efficiencies but maintaining the economic and environmental cost advantages of thin-film deposition techniques [7]. These include multiple junction devices, combining materials responding to different spectral regions, mirror/lens based concentrators to increase the level of light exposure of the device, up to the equivalent of hundreds of suns and organic polymer and dye-sensitized devices, based on very low cost technology and available on flexible substrates [16]. Third generation also covers a new class of thin film solar cells currently under investigation, the perovskite solar cells, which show huge potential with record efficiencies beyond 20% on very small area [15]. Although the performance and stability of third generation solar cells is still limited compared to first and second generation solar cells, they have great potential and are already commercialized [15]. Figure 7 shows the efficiency versus costs of the three PV generations.

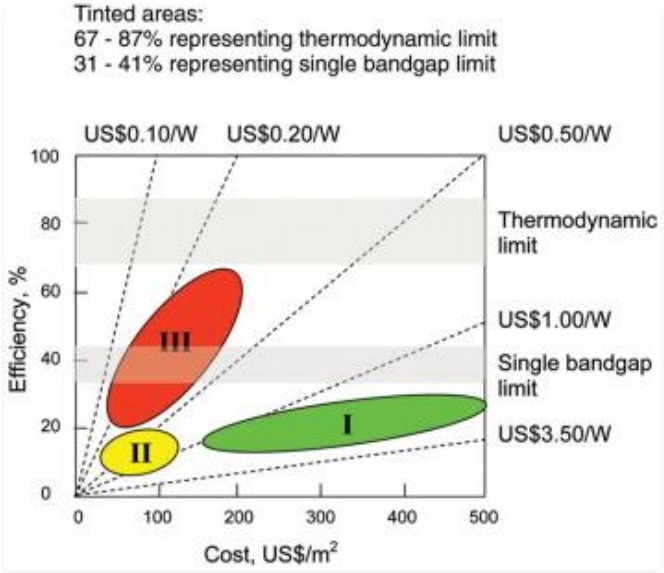

Figure 7. Efficiency and cost projections for first- (I), second- (II), and third-generation (III) PV technologies (wafer based, thin-films and advanced thin films, respectively) [7].

Thereby, there are three main focuses in the research and development of solar cell technologies: increasing the efficiency, reducing the production cost, and expanding the application coverage area. As seen, there are multiple factors that affect the behavior of the semiconductor material and thus the efficiency of the solar cells. Therefore, it becomes necessary to optically and electrically characterize solar devices, regardless of the technology used, in order to optimize their operation. In practice, the two techniques most widely used to measure the efficiency of solar cells are maximum power point tracking and quantum efficiency methods [17]. A correct characterization with different experimental methods, such as those that will be explained later, allows a follow-up of the production processes, opening the possibility to tackle the technological challenges that are currently being sought.

1.5. Scope of the present work

Currently there are different techniques for characterizing solar cells, whose purpose is their electrical, optical and structural evaluation. These techniques allow not only an integral characterization of the device, but also enable the evaluation of intermediate manufacturing steps to achieve optimum performance of the solar cells. The objectives of this work are presented below:

- Assembly and commissioning of the experimental system at the Optics Laboratory in Universidad de La Laguna, comprising the equipment for External Quantum Efficiency measurement and Solar Simulator.

- Evaluation of the spectral response of the solar cells by quantum efficiency measurements and verification of the validity of the results obtained.

- Electrical characterization using a Solar Simulator that reproduces the standard solar spectrum AM1.5G to obtain the current-voltage (I-V) and power-voltage (P-V) curves. This will allow the determination of the characteristic parameters of solar devices. Likewise, a method for measuring and obtaining the parameters that will enable systematical and optimal characterization of solar devices is developed.

2. Fundamentals

The most important parameters that describe the performance of solar cells are the spectral distribution of the irradiance, total irradiance and temperature [14]. Thus, it is clearly desirable to obtain PV devices that respond to as much of the broad source emission range as possible and have maximum conversion efficiency. However, in practice, devices only respond to a restricted range of wavelengths, limited at long wavelengths by the material band gap, and at short wavelengths by material absorption [16].

2.1. Spectral Response *(SR)* mathematical description

The spectral response is a key parameter for silicon solar cells since it is the sensitivity of a solar cell corresponding to light of different wavelengths while it is a measurement of short circuit current per incident light power unit in general [18]. This measurement is performed by shining a monochromatic probe beam onto the sample and registering the photocurrent generated as a function of wavelength [16].

Device spectral response depends upon a large number of factors, including material system, device design, electrical contact, etc. Additionally, for single junction devices is limited by the Shockley-Queisser limit [16].

The SR of a solar cell is calculated by dividing its photocurrent reading (*Isc)* with the power of monochromatic beam (Pinc) or the intensity of the incident radiation (*Iinc*) of incident area (*Ainc*), as

$$SR(\lambda) = \frac{I_{sc}(\lambda)}{P_{inc}(\lambda)} = (A_{inc})^{-1}\frac{I_{sc}(\lambda)}{I_{inc}(\lambda)} \quad [A/W] \tag{3}$$

2.2. External Quantum Efficiency *(EQE)* mathematical description

The external quantum efficiency is defined as the number of charge carriers collected by the solar cell per photon incident on the device, and can be directly obtained from the spectral response measurement [16].

$$EQE(\lambda) = \frac{I_{sc}(\lambda)/q}{P_{inc}(\lambda)/E_{\lambda}} = \frac{hc}{q\lambda} SR(\lambda) \quad (4)$$

Where q is the charge of one electron, E_{λ} is the energy of one photon, h is Planck's constant, c is the speed of light and λ is the wavelength.

The measurement of the EQE as a function of the wavelength is a valuable indicator of the conversion of solar radiation into electricity, which helps the researcher to observe and identify solar cell's characteristics in the particular range of wavelength of incident light [6].

In principle, an ideal solar cell should have high spectral response for wavelengths where a large number of incident photons exist and the minority carriers produced are collected. However, phenomena such as surface recombination, small diffusion lengths and reflections come into play, resulting in efficiency losses. Additionally, for the incident photons whose energy is lower than the bandwidth, the quantum efficiency will be equal to zero [17]. Annex A.1. shows the main conversion efficiency losses with respect to an ideal solar cell.

2.3. Internal Quantum Efficiency *(IQE)* mathematical description

The EQE considers optical losses by transmission and reflection in the solar cell, but it can be modified to take into account only the portion of the incident light reaching the active region, to yield the internal quantum efficiency. This allows a better understanding of the material properties of the device [16].

Therefore, IQE is defined as the number of absorbed photons in the solar cell to the number of collected carriers.

$$\mathrm{IQE}(\lambda) = \frac{\mathrm{EQE}(\lambda)}{1 - \mathrm{R}(\lambda)} \quad (5)$$

Where R(λ) is the reflectance of the solar cell, being assumed that the transmittance T(λ) is null. IQE informs about the fraction of absorbed photons that are being converted to electrons in the device. In general, IQE is always higher than EQE for a given device because the factor 1-R is always less than 1.

2.4. Photovoltaic cell Current-Voltage (I-V) mathematical description

To electrically characterize a device, the conduction mechanisms must be evaluated when the device is exposed to optical energy. To do this, the properties of the cell are evaluated by intensity measurements based on the applied voltage, obtaining the so-called I-V characteristics that allow relating the properties of solar cells with the ability to transform optical energy into electrical energy

[6]. The current-voltage (I-V) and power-voltage (P-V) curves are critical in the analysis of a solar cell's output performance and solar efficiency.

The electric current supplied by an ideal solar cell to a load is given by the difference between the photocurrent I_L, which depends on the incident flow of photons, and the recombination or diode current I_D, due to the polarization produced by the generated voltage. This equation can be expressed by [9]:

$$I = I_L - I_D = I_L - I_0 \left[e^{\left(\frac{V}{mVt}\right)} - 1 \right] \quad (6)$$

Where I_0 is the darkness current and V_T is the thermal voltage equal to *kTc/q*, (1<m <2, is an ideality factor lacking physical meaning with m = 1.3 for Silicon, K is the Boltzmann constant, q is the electron charge and Tc is the absolute temperature). The previous equation can be written as a function of the short circuit current, $I_{SC} \equiv$ I (V=0) and the open circuit voltage, $V_{OC} \equiv$V (I=0), as follows:

$$I = I_{sc} \left[1 - e^{-\frac{(Voc - V)}{mVt}} \right] \quad (7)$$

Nevertheless, in a real solar cell there are other effects not considered in the former equation that affects the external behaviour of the solar cell; the series resistance (R_S) which owes its origin to the resistance of the metallic contacts with the semiconductor, and the parallel resistance (R_P) that can be due to leakages of current by the surface of the edges of the cell, among other effects.

In the commercial solar cells studied we have only taken into account, in some cases, the series resistance. If we consider the effects of the parallel resistance as negligible and the photogenerated current is equal to the short circuit current, we can get to the expression we have used [9]:

$$I = I_{sc} \left[1 - e^{\frac{(V - Voc + IRs)}{mVt}} \right] \quad (8)$$

Where it is assumed that Voc >> Isc Rs.

Within a wide operating range, the photocurrent of the practical solar cells is directly proportional to the intensity of the incident radiation (Ei) and independent of the applied voltage, and the open circuit voltage (Voci) changes according to:

$$V_{ocj} = V_{oci} + mV_t \ln\left(\frac{E_j}{E_i}\right) \quad (9)$$

Where it has been presumed that the photocurrent is much greater than the saturation current.

The influence of temperature is very small in the generation of carriers; however, by introducing typical values of the silicon, the influence of the temperature on the open circuit voltage reaches the value:

$$\frac{dV_{oc}}{dT_c} = -2{,}3 \text{ mV/°C} \quad (10)$$

This equation indicates that Voc decreases at a rate of 0.4% for each degree that increases the temperature.

Annex A.2, showing a generic I-V curve of a standard solar cell under illumination, reveals the existence of a maximum power point, P_{MPP}, defined by the current and voltage at this point, I_{MPP} and V_{MPP}, respectively. Its location can be approached using an approximate analytical solution, given by [9]:

$$I_{MPP}/I_L = 1 - a^{-b} \quad (11)$$

$$V_{MPP}/V_{OC} = 1 - \ln a \,/a \quad (12)$$

Where

$$a = 1 + \ln\left(\frac{I_L}{I_0}\right)$$

$$b = a/(a+1) \quad (13)$$

Notably, the FF is an indication of internal losses that is visually communicated by how much the I-V characteristic curve deviates from a rectangular shape in the shown quadrant (annex A.2). In practice, it is a widely used parameter given its little variation from one device to another and the fact that it remains reasonably constant when varying operating conditions.

$$FF = \frac{I_{MPP}V_{MPP}}{I_{SC}V_{OC}} \quad (14)$$

The concept of energy conversion efficiency of a solar cell is also widely used, understood as the relationship between the electrical power it can deliver and the light power it receives [9]. That is:

$$\eta \equiv \frac{I_{MPP}V_{MPP}}{P_{inc}} \equiv \frac{FFI_{SC}V_{OC}}{P_{inc}} \quad (15)$$

3. Experimental details

3.1. Spectral Response and External Quantum Efficiency Measurement

The experimental setup used in the ULL optics laboratory is shown in Figure 8. The EQE measurement system consists of a source (Xe, W lamps), a monochromator (MS257TM ¼ m), the optics used to focus the beam on the sample (5-7 of Figure 8), the device under test (DUT) (8) and the detection and analysis system (9-10 of Figure 8). Annex A.3 shows the measurement equipment described.

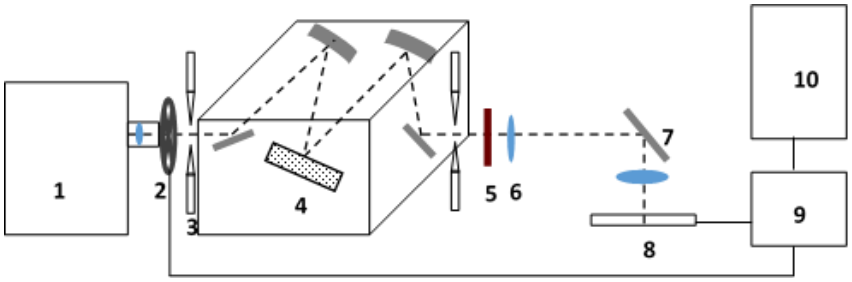

Figure 8. EQE experimental setup diagram. (1) Xe or W lamp; (2) Chopper; (3) slit; (4) grating; (5) optical filter; (6) lens; (7) mirror; (8) solar cell, photodetector; (9) lock-in amplifier and (10) computer.

The measurement procedure employed to obtain the EQE is the reference cell method [19]. This method consists of using a reference cell from which the spectral response is known (SRref). If we measure the photogenerated current (Iref out) and the area of the incident light (Aref) is known, by equation (3) we have,

$$SR_{ref} = \left(A_{ref}\right)^{-1} \frac{{I_{ref}}^{out}}{{I_{ref}}^{inc}} \tag{16}$$

If we now measure the photogenerated current of the device under test (DUT), (I_{DUT} out), and the area of the incident light (A_{DUT}) is known, we have,

$$SR_{DUT} = (A_{DUT})^{-1} \frac{{I_{DUT}}^{out}}{{I_{DUT}}^{inc}} \tag{17}$$

As the incident power can only change if the incident light area changes over the sample, we can write,

$$\begin{aligned} {I_{DUT}}^{inc} &= {I_{ref}}^{inc} \\ SR_{DUT} &= \left(\frac{A_{ref}}{A_{DUT}}\right)\left(\frac{{I_{DUT}}^{out}}{{I_{ref}}^{out}}\right) SR_{ref} \end{aligned} \tag{18}$$

In the case that $A_{DUT} > A_{ref}$, the SR will be greater than expected and it would have to be multiplied by a factor A_{ref} / A_{DUT} <1. Conversely, if $A_{DUT} < A_{ref}$, the SR will be lower than expected and would have to multiply by a factor A_{ref} / A_{DUT} >1. If $A_{DUT} = A_{ref}$, the multiplication factor will be 1.

On the other hand, in order to contrast the results of the afore mentioned method, as well as the data provided by the manufacturer, measurement of EQE was performed at ITER by means of the Spectral Response Characterization System Bentham PVE300, shown in Figure 9.

For the measurement of spectral response (SR) and external quantum efficiency (EQE) with this equipment the sample under test is mounted horizontally on a temperature controlled vacuum mount for thermal stability. A monochromatic probe beam is made to be incident upon the sample under test and the photocurrent generated by the device is measured at each wavelength. Having previously measured the power in the beam with two detectors of known responsivity, a Silicon photodiode for wavelengths ranging from 300 to 1000 nm and Germanium for 800 to 1800 nm, SR and EQE of the desired device can be directly obtained.

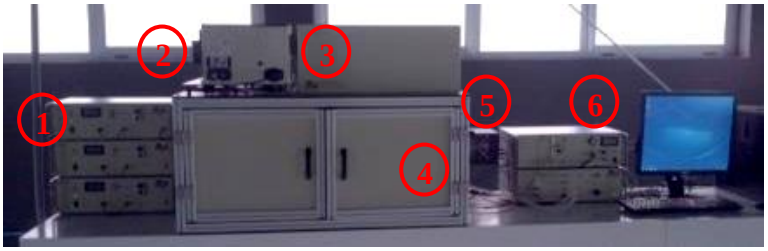

Figure 9. Bentham PVE300. (1) Constant current lamp power supplies; (2) Xe and QH sources; (3) TMc300 monochromator; (4) Process chamber; (5) Solar simulator with six-fibre bundle and (6) *(above)* Detection electronics unit and *(below)* vacuum chuck controller.

The equipment comprises three constant current power supply (1) required for each light source (xenon, quartz halogen and solar simulator). The stability of these units ensures constant light output.

The dual light housing (2) is composed of xenon and quartz halogen light sources, which provide optimum illumination from the UV to the NIR. A swing away mirror (SAM) is coupled between them to permit selection as a function of wavelength. The dual source is fitted with an optical chopper to provide an AC probe signal. Both the output of the Xenon lamp and that of QH are coupled to the monochromator via an off-axis parabolic reflector for the former and condenser lenses for the latest.

A 300 mm focal length monochromator (3) is installed with a Czerny-Turner configuration, which uses two plane diffraction gratings. A mirror-based relay optic is employed to image the output of the monochromator at the sample plane. An aperture box is attached to the exit slit.

The process chamber (4) contains the transformer and the temperature controlled vacuum mount with probes, which provides a convenient mounting of electrical probing and allows controlling sample temperature by a quartet of Peltier devices accompanied by the control unit. Annex A.4 shows an interior view of the process chamber.

The bias source is provided by the solar simulator (5) consisting of a variable intensity quartz halogen lamp with computer controlled shutter. Light is transported via six-branch fibre to ensure uniform illumination in the sample plane.

The detection electronics housing (6) comprises an optical chopper to provide an AC probe beam and two lock-in amplifiers to account for phase variations throughout the scan and recover the optically chopped signal. Finally, the vacuum chuck controller (6) ensures stable sample temperature to counter the heating effects attendant to use of a solar simulator. The control unit contains the vacuum and water pumps and the bi-polar temperature control electronics [20].

3.2. Internal Quantum Efficiency Measurement

Internal quantum efficiency measurement was performed at SiCell laboratory in ITER, using the fluorometer, also referred to as spectrometer. In this equipment's configuration, both the excitation and emission channels consist of two monochromators. It also incorporates an integrating sphere coated with Barium Sulphide, a highly diffusely reflecting material.

Measurement of sample reflectance is made with respect to a reference standard of reflectance, which calibrate the system against a presumed reference level of 100%. A silicon photo-diode is used as reference detector, receiving a small percentage of reflected light, while the majority of light is transmitted to the sample.

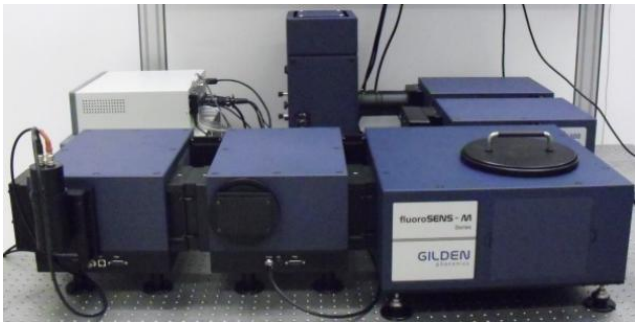

Figure 10. Fluoro Sens M-Series Fluorimeter with dual monochromator system from Gilden Photonics.

3.3. Current-Voltage (I-V) Measurement

The experimental setup used in the ULL optics laboratory is shown in Figure 11. This I-V measurement system consists of a source (Xe lamp), spectrum shaping elements, for instance the AM 1.5G filter (2 of Figure 11) (annex A.5), the device under test (DUT) (6) and the measurement system (7 of Figure 11) consisting of 6517A electrometer (annex A.6). Annex A.7 shows the measurement equipment described in Figure 11.

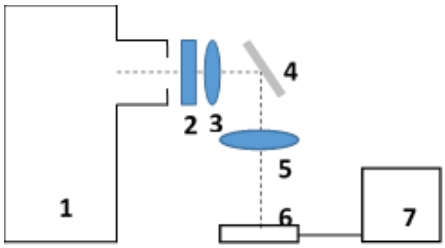

Figure 11. I-V experimental setup diagram. (1) Xe lamp; (2) Solar filter; (3,5) lenses; (4) mirror; (6) solar cell and (7) electrometer.

Measurement of the I-V curve was conducted to obtain the parameters that define solar cells' behavior, that is, short-circuit current, open circuit voltage, current density, maximum power output, fill factor (FF), efficiency and series resistance. The experimental procedure followed was:

1. Checking the electrometer, by measuring a current voltage characteristic in a resistance.

2. Measurement of irradiation (Tes-1333 Solar Power Meter) obtained with the solar simulator when the cell is fully illuminated.

3. Measurement with the electrometer of the intensity and voltage supplied according to the circuit of Annex A.8.

4. The experimental data obtained by the theoretical curve characteristic according to the equation (7 or 8) are adjusted by the Levenberg-Marquardt algorithm. We get the short circuit current and open circuit voltage under experimental conditions.

5. Assuming linear the dependence between the short circuit current and the irradiation, we calculate the new short circuit current and the open circuit voltage at 1 sun according to equation (9).

6. Finally we calculate the current voltage characteristic at 1 sun.

The value of $J_{sc} = I_{sc}/A_{inc}$ can be used to validate the EQE or SR measurement result based on equations (3) and (4) by means of

$$J_{sc} = q\int \phi(\lambda)\bullet EQE(\lambda)d\lambda = \int E_0(\lambda)\bullet SR(\lambda)d\lambda \quad (19)$$

Where q is the charge of the electron, ϕ is the incident photon flux and E_0 is a standard reference of solar spectral irradiance according to ASTM G173-03 [12], as we show in Figure 6.

This calculation however assumes that the EQE used is representative of the entire cell. If significant variation in performance over the cell area is present, the calculated J_{sc} will not be representative. There are several factors that could lead to incorrect estimation of the EQE such as the different spectral response between the reference cell (which is often used to determine the irradiance of the solar simulator) and the measured cell. All photons reaching a solar cell are not transmitted only to the active region where the conversion process occurs.

4. Results and discussion

Different devices have been used to measure the magnitudes involved in the photogeneration of current of solar cells. Tests were conducted on a reference mono-crystalline silicon cell, a GaAsP photodetector and various devices based on mono-crystalline silicon technology.

4.1. EQE measurement

As described in section (3.1.) above, a photodetector of known responsivity, referred to as Rera, has been employed as reference cell, which will serve to obtain the external quantum efficiency of various devices. This mono-crystalline silicon reference cell is a high-quality sensor for the determination of solar simulator irradiance levels. The cell's calibration was performed against an established set of reference cells calibrated at NREL (National Renewable Energy Laboratory) and Fraunhofer Institute for Solar Energy Systems (ISE).

Figure 12. Mono-crystalline reference cell from Rera Solutions.

- **Mono-crystalline reference cell Rera**

The results obtained at ITER by means of the PVE300 characterization system are presented against the manufacturer's data. For future determination of the EQE of different devices, the outcome of this cell will be used as reference.

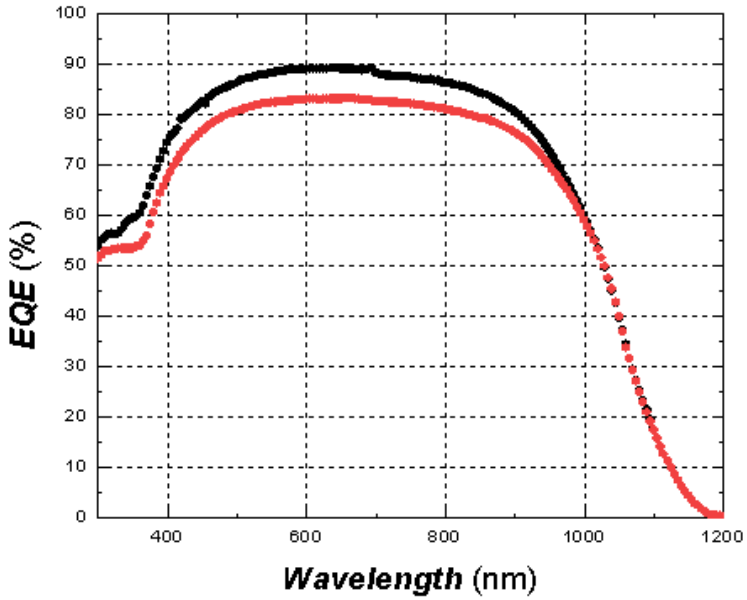

Figure 13. *(Red dots)* EQE provided by manufacturer. *(Black dots)* EQE measured with Bentham PVE300 at ITER

As can be seen in Figure 13, photons whose energy is less than a wavelength corresponding to 400 nm are absorbed in the first microns of the solar cell, leading to a reduced response due to front surface recombination. The spectral region in the range of 950-1000 nm is affected by rear surface recombination. The response for wavelengths greater than 1000 nm is due to the internal reflection of the back surface of the solar cell but is affected by a reduced absorption and low diffusion lengths. At long wavelengths, i.e. 1200 onwards, the EQE is zero given that no light is absorbed below the band gap. Finally, a reduction from the overall ideal conversion efficiency is caused by reflection and low diffusion lengths. In general, a typical behavior for c-Si cells is observed.

Employing the procedure described at paragraph (3.1), we successfully carried on with the determination of the EQE of various devices using the EQE data of the reference cell Rera

experimentally obtained at ITER. Tests were performed at the Optics Laboratory in ULL employing a Wolfram lamp in the range 300 to 1100 nm as it was proven to obtain more accurate results.

Results with very good approximation to the data of the manufacturer were obtained, proving the feasibility of the SR measurement system built at the ULL Optics Laboratory. The outcome of a mono-crystalline silicon cell and a GaAsP photodiode is presented below and compared with the manufacturer's technical information.

- **XOB17-12x1**

The solar cell XOB17-12x1 from IXYS is composed by a single coated mono-crystalline silicon cell with dimensions 22x7x1.6 mm.

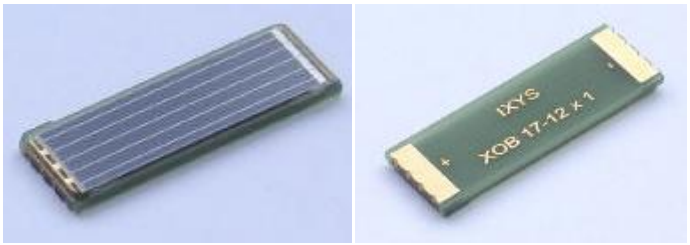

Figure 14. Front and back-side view of XOB17-12x1 cell.

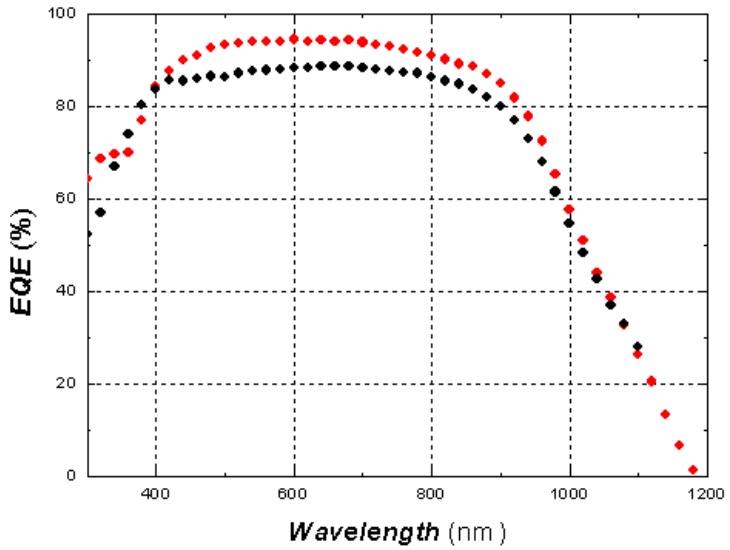

Figure 15. *(Red dots)* EQE of XOB17-12x1 provided by manufacturer. *(Black dots)* EQE obtained by the reference cell method

The result shows a typical behaviour of a mono-crystalline silicon cell. SR and EQE of this device were measured with a small error as can be seen from the curve provided by the manufacturer, therefore confirming the feasibility of the experimental setup and validating the reference cell method employed.

- **G2119 GaAsP photodiode**

The GaAsP photodiode from Hamamatsu, with reference G2119, is a photosensor with suppressed sensitivity in the long wavelength range compared to Si photodiodes, with a spectral response close to the human eye sensitivity. It is composed by a single photosensor with an area of 10.1x10.1 mm.

Figure 16. G2119 GaAsP photodiode from Hamamatsu.

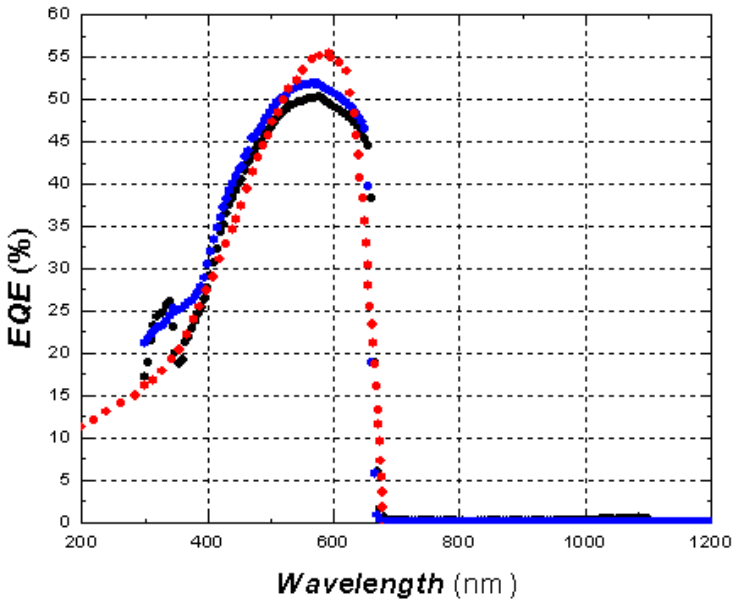

Figure 17. *(Red dots)* EQE of G2119 GaAsP photodiode provided by manufacturer. *(Black dots)* EQE obtained by the reference cell method *(Blue dots)* EQE measured with Bentham PVE300 at ITER

Figure 17 shows a typical behaviour for this type of detector. It has suppressed sensitivity in the long wavelength range but is useful for detection of UV-VIS radiation. The spectral bandwidth of the response ranged from 200 to 680 nm, with a peak response at around 580 nm for the experimental results.

Measurement with the spectral response characterization system Bentham PVE300 shows good agreement with that applying the reference cell method, which proves the feasibility of this method. Both results show a good approximation of the manufacturer's data.

4.2. IQE measurement

The test was performed in three different devices: a mono-crystalline silicon cell with printed metallic front-contacts, a mono-crystalline silicon cell with gridlines only in the back of the cell from Sun Power, and a multi-crystalline silicon cell also with metallic front contacts.

- **Mono-crystalline cell**

The results of the mono-crystalline cell of 50x50 mm, shown in Figure 18, are presented below.

Figure 18. Mono-crystalline Silicon cell of 50x50 mm with printed metallic front contacts.

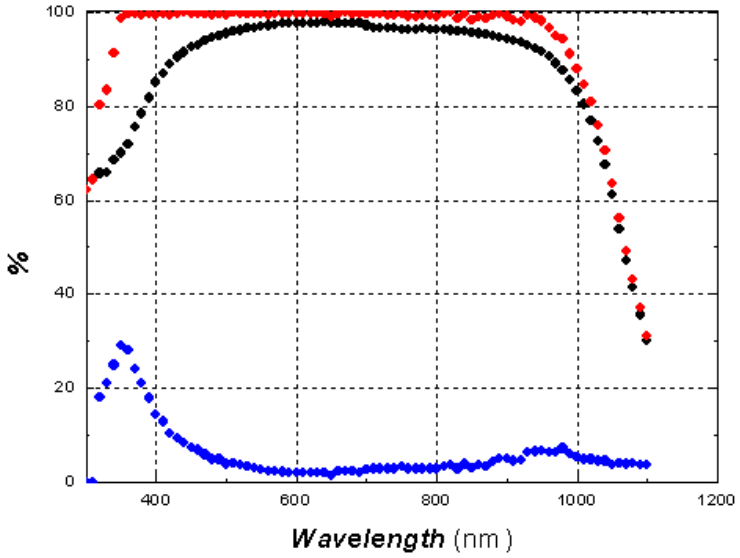

Figure 19. *(Red scatter)* IQE of the mono-crystalline silicon cell experimentally obtained. *(Black scatter)* EQE measured with Bentham PVE300 at ITER. *(Blue scatter)* Reflectance experimentally obtained with the spectrometer Fluoro Sens.

For the measurement, both data of EQE and reflectance were obtained at the SiCell lab in ITER. EQE measurement was performed by means of the Spectral Characterization System Bentham PVE300, while reflectance was acquired with the spectrometer Fluoro Sens.

In order to take into account the difference of the incident angle of the beam in both measurements, reflectance has been adjusted so as to consider an angle of 0º between the beam and the sample, since the test was performed at 45º. This was achieved by the Schlick's approximation as follows [21]:

$$F(\theta) = F(0) + \big(1 - F(0)\big)(1 - \cos\theta)^5 \qquad (20)$$

Where *F(θ)* is the reflectance obtained at 45º and *F(0)* the reflectance at 0º. IQE was then simply calculated by applying equation (5).

- **Sun Power mono-crystalline silicon cell**

As for the mono-crystalline Silicon cell from Sun Power, the distinctiveness of this device is the all-back contact cell design, which moves gridlines to the back of the cell, leaving the entire front surface expose to sunlight.

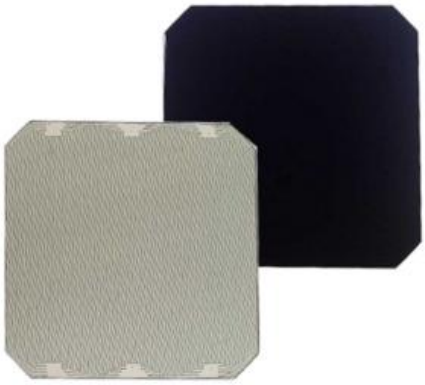

Figure 20. Mono-crystalline C60 Solar Cell from Sun Power. The all-back contact design, moves gridlines to the back of the cell.

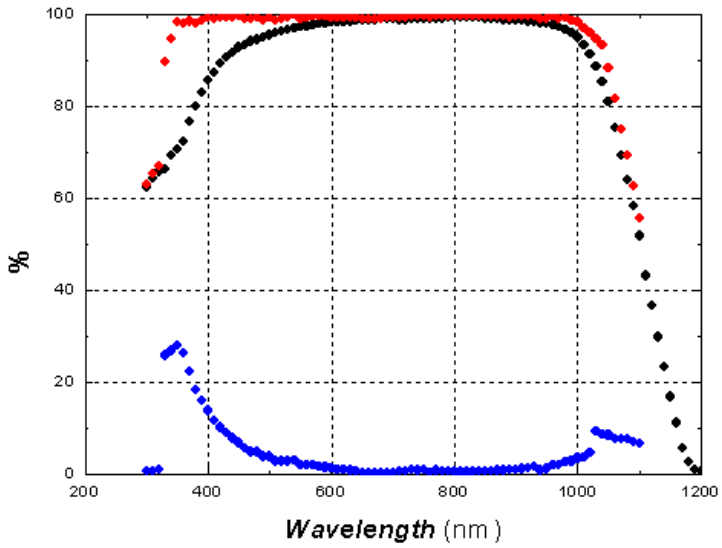

Figure 21. *(Red scatter)* IQE of the mono-crystalline silicon cell C60 from Sun Power experimentally obtained. *(Black scatter)* EQE measured with Bentham PVE300 at ITER. *(Blue scatter)* Reflectance experimentally obtained with the spectrometer Fluoro Sens.

Surface reflectance of this cell presents lower values in the range of 400 to 1000 nm in comparison with the previously mono-crystalline cell (Figure 18). This is precisely the desired behaviour, indicating a good anti-reflective layer quality, or an advantage in the innovative design with rear gridlines.

- **Multi-crystalline silicon cell**

Finally, results of the multi-crystalline silicon cell are presented below.

Figure 22. Multi-crystalline silicon cell with dimensions 125x125 mm.

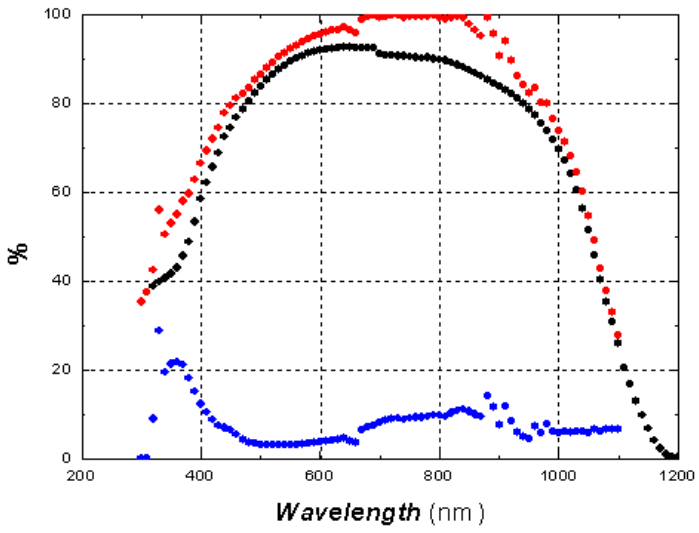

Figure 23. *(Red scatter)* IQE of the multi-crystalline silicon cell experimentally obtained. *(Black scatter)* EQE measured with Bentham PVE300 at ITER. *(Blue scatter)* Reflectance experimentally obtained with the spectrometer Fluoro Sens.

The reflectance, which is the base quantity that characterizes the process of reflection, is defined as the ratio of the reflected radiant flux (or power) to the incident radiant flux (or power) [22], and at any wavelength λ can be considered to be the sum of two components: regular (or specular, or mirror) reflectance and diffuse (or volume, or non-directional) reflectance [23].

This parameter is used to indicate the quality of the anti-reflective (AR) layer deposited on the surface of a silicon-based wafer. As it can be observed from the results, a minimum reflectance for the optimal wavelengths for the performance of solar cells is sought. Although the three measured cells showed a reflectance within the usual values, the best result was found in the mono-crystalline C60

solar cell from Sun Power, presumably due to the all-back contact design, which avoids surface reflections caused by the metallic gridlines on the front.

4.3. I-V measurement

Measurement of the I-V characteristic of various devices was performed at the optics laboratory at ULL. The set-up and procedure described at paragraph (3.2.) were followed, achieving appropriate results in the different devices studied.

- **Mono-crystalline reference cell Rera**

Results of the mono-crystalline reference cell Rera are presented below and analyzed against the manufacturer's technical information (Table 1).

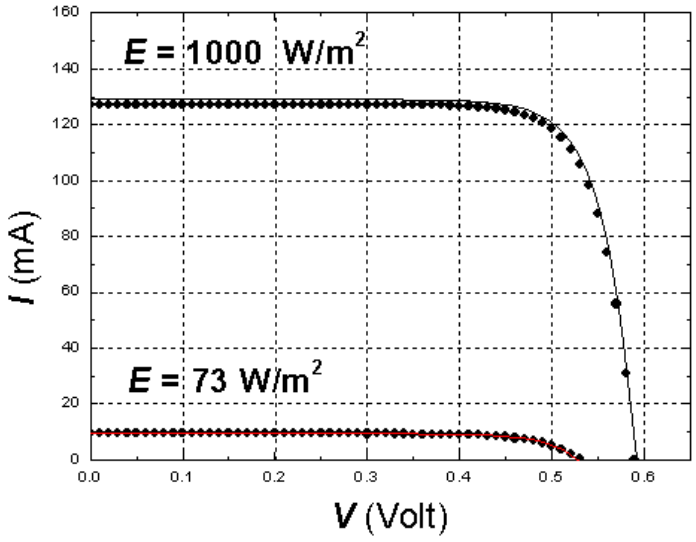

Figure 24. *(Scatter)* I-V characteristic of the reference cell Rera at experimental conditions with an irradiance of 73 W/m² and simulated for an irradiance of 1 sun. *(Red line)* Theoretical curve adjusted. *(Black line)* Manufacturer's I-V characteristic.

Under experimental conditions, the theoretical curve characteristic according to equation (8) is adjusted employing the Levenberg-Marquardt algorithm, yielding a value of Voc and Isc of 0.53 V and 9.28 mA, respectively. Additionally, a series resistance of 0.2Ω is obtained.

To extrapolate the experimental data to an irradiance of 1 sun, a linear relationship between the short circuit current and the irradiation is assumed. As for the open circuit voltage, equation (9) has been considered. Thereby, theoretical values of Voc and Isc under STC are obtained, being these 0.61 V and 127.15 mA, in accordance with the manufacturer's technical information (see Table 1). The cell's I-V characteristic simulated at 1 sun was obtained in accordance to equation (8).

Below are the results corresponding to the power curve of the reference cell presented against the manufacturer's data.

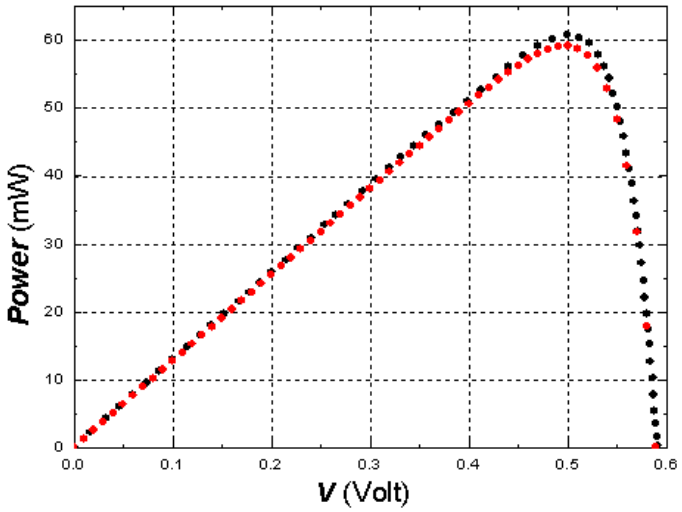

Figure 25. *(Black dots)* Power curve of the reference cell Rera provided by the manufacturer. *(Red dots)* Power curve experimentally obtained.

- **XOB17-12x1**

With respect to the mono-crystalline cell XOB17-12x1, same methodology as formerly explained was undertaken. The theoretical curve characteristic was first adjusted according to equation (7) and to equation (8) afterwards, in order to account for the series resistance effects. An active area of 1.2 cm² was considered in the calculations. Table 1 shows the test results compared with the manufacturer's technical information.

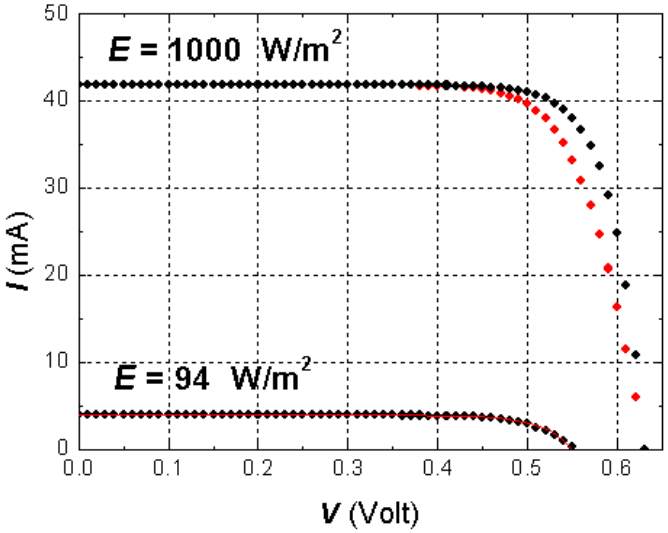

Figure 26. *(Black Scatter)* I-V characteristic of the mono-crystalline cell XOB17-12x1 at experimental conditions with an irradiance of 94 W/m² and simulated at 1 sun with no series resistance. *(Red Scatter)* I-V characteristic simulated at 1 sun with a series resistance of 0.8 Ω. *(Red line)* Theoretical curve adjusted.

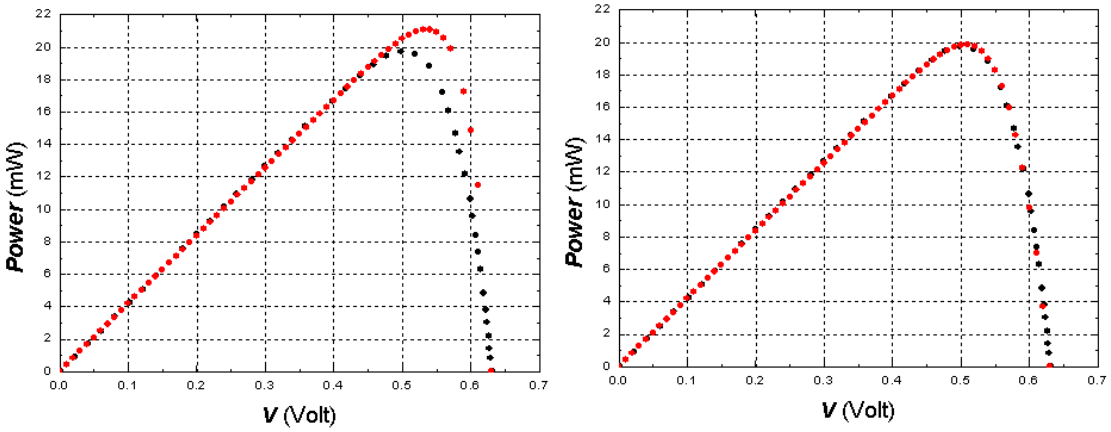

Figure 27. Left. *(Black dots)* Power curve of XOB17-12x1 provided by the manufacturer. *(Red dots)* Power curve theoretically obtained with no series resistance. **Right.** *(Black dots)* Power curve provided by the manufacturer. *(Red dots)* Power curve theoretically obtained with a series resistance of 0.8 Ω.

In **Figure 27. Left**, the discordance between both power curves is presumably due to the effect of the series resistance at 1000 W/m², since it varies with the irradiance. Therefore, to experimentally reproduce the manufacturer's I-V characteristic, the effect of this series resistance should be considered. At experimental conditions the series resistance was practically null, while at the simulations at 1 sun a resistance of 0.8 Ω was found. **Figure 27. Right** shows good agreement with the manufacturer's curve when this resistance is considered.

The test was performed on two other devices, both based on mono-crystalline silicon technology, namely KXOB22-01x8F and SLMD480H12L. The results are presented in Table 1 together with the technical information of both modules.

- **KXOB22-01x8F**

The device KXOB22-01x8F is composed by 8 cells in series with a unit cell size of 5x2.4 mm and of 22x7x1.8 mm altogether. The wafer active area is 0.104 cm².

Figure 28. Front and back-side view of KXOB22-01x8F.

In this case, as it is a module instead of a single solar cell, the generic I-V curve of the device should account for the number of cells connected in series, N, being as follows [23]:

$$I = I_{sc}\left[1 - e^{-\frac{(Voc-V)}{NmVt}}\right] \quad (21)$$

Likewise, assuming constant temperature, for a different irradiance Ej, the variation of the open circuit voltage (Vocj) changes accordingly to [23]:

$$V_{ocj} = V_{oci} + NmV_t \ln\left(\frac{E_j}{E_i}\right) \quad (22)$$

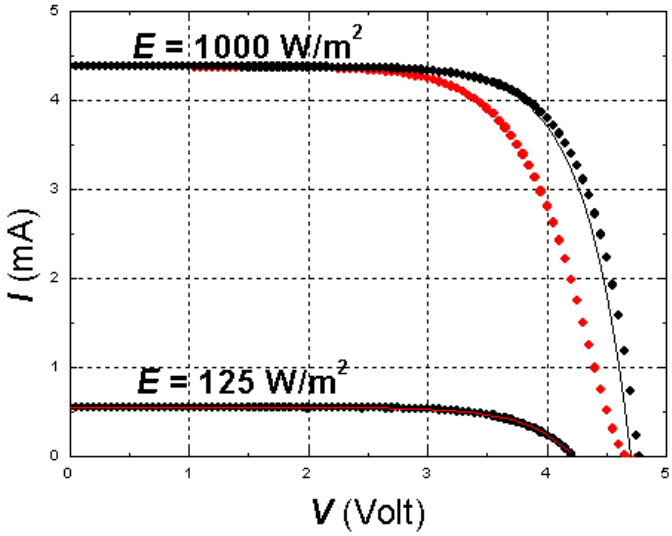

Figure 29. *(Black Scatter)* I-V characteristic of the module KXOB22-01x8F at experimental conditions with an irradiance of 125 W/m² and simulated for an irradiance of 1 sun with no series resistance. *(Red Scatter)* I-V characteristic simulated at 1 sun with a series resistance of 100 Ω. *(Red line)* Theoretical curve adjusted. *(Black line)* Generic I-V curve with manufacturer data (no series resistance added).

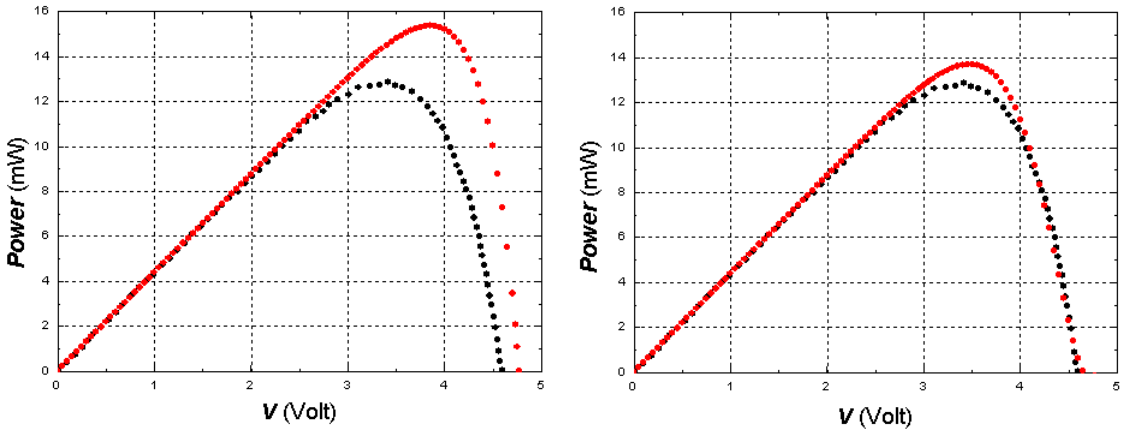

Figure 30. Left. *(Black dots)* Power curve of KXOB22-01x8F provided by the manufacturer. *(Red dots)* Power curve theoretically obtained with no series resistance. **Right.** *(Black dots)* Manufacturer's P-V curve. *(Red dots)* Power curve theoretically obtained with R_S = 100 Ω.

In this case, a slight deviation in the Voc experimentally obtained leads to a greater deviation in the calculated power curve (Figure 30. Left). Again, the series resistance plays a determining role since, not being considered in the simulation at 1000 W/m², increases the theoretical Voc against the value provided by the manufacturer. The model with R_S = 100 Ω was applied, resulting in a good approximation of the manufacturer's P-V curve, as seen in **Figure 30. Right**.

Although a priori it seems an excessive value for R_S since it is intended to be as low as possible, we must consider that it is a module with 8 cells in series, so the unit value per cell will be 12.5 Ω.

- **SLMD480H12L**

As for the SLMD480H12L mini module, it comprises 12 cells in series, with a unit cell size of 10x4.8 mm and of 22x35x2 mm altogether. The active area of this device is 5.83 cm².

Same considerations as in the former device has been assumed, with N=12. However, no series resistance was found to be necessary.

Figure 31. Front and back-side view of SLMD480H12L.

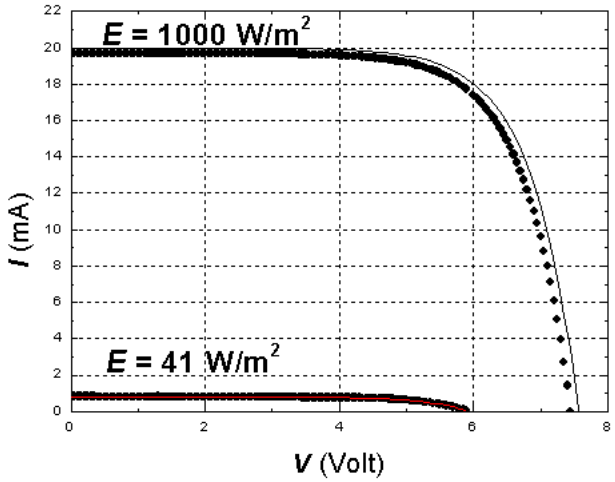

Figure 32. *(Scatter)* I-V characteristic of the mono-crystalline module SLMD480H12L at experimental conditions with an irradiance of 41 W/m² and extrapolated to an irradiance of 1 sun. *(Red line)* Theoretical curve adjusted. *(Black line)* Manufacturer's I-V characteristic.

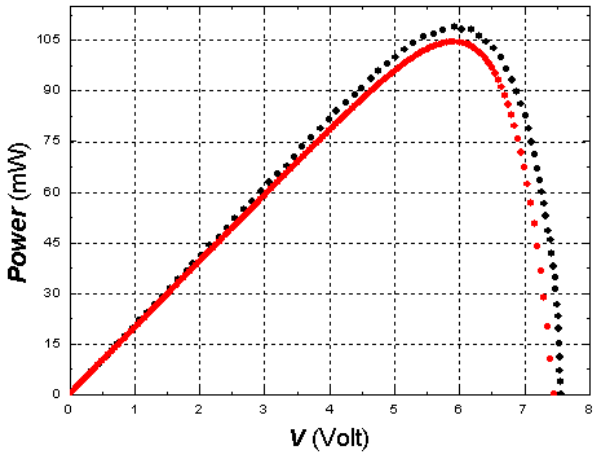

Figure 33. *(Black scatter)* Power curve of SLMD480H12L provided by the manufacturer. *(Red scatter)* Power curve experimentally obtained.

4.4. Cells characteristic parameters

From the I-V characteristic of each device short circuit current, open circuit voltage, current and voltage at the maximum power point, fill factor and efficiency were obtained.

To extract I_{SC} under STC a linear relationship between the short circuit current and the irradiation was considered. As for V_{OC}, equation (9) or (22) was employed, depending on whether it was a single solar cell or a module.

The parameters I_{MPP} and V_{MPP} were verified by mean of equations (11) and (12) to subsequently extract the fill factor (FF) and conversion efficiency of the solar devices employing equations (14) and (15), respectively.

To obtain the short circuit current density, J_{SC}, equation (19) was used, for which the solar spectral irradiance according to ASTM G173-03 [12] was employed. The spectral response as a function of wavelength was achieved by means of the EQE measurement equipment built at the ULL Optics Laboratory.

Cells Parameters	***RERA*(1)**		***XOB17-12x1*(2)**		***KXOB22-01x8F*(3)**		***SLMD 480H12L*(4)**	
	Data Sheet	*Test Results*	*Data Sheet*	*Test Results*	*Data Sheet*	*Test Results*	*Data Sheet*	*Test Results*
Isc (mA)	129	127.15	42	41.85	4.4	4.38	20	19.69
Voc (V)	0.591	0.6147	0.63	0.6289	4.7	4.77	7.56	7.45
Impp (mA)	122	118.38	39	38.9	3.8	3.9	18	17.72
Vmpp (V)	0.499	0.5	0.51	0.51	3.4	3.5	6.06	5.9
Jsc (mA/cm²)	32.3	33.7	35	34.06	42.4	36	42.4	36.1
FF (%)	79.9	75.7	> 75	75.4	> 60	65.3	> 70	71.3
η (%)	15.2	14.8	17	16.56	22	18.5	22	18.2

Table 1. Manufacturer's technical information and experimental results extracted from the I-V characteristic curve and EQE measurements of the different devices studied.

(1) https://www.rerasolutions.com/product/silicon-reference-cell/
(2) http://ixapps.ixys.com/datasheet/xob17-solar-bit-datasheet_mar-2008.pdf
(3) http://ixapps.ixys.com/DataSheet/KXOB22-01X8F_Nov16.pdf
(4) http://ixapps.ixys.com/DataSheet/SLMD480H12L_Nov16.pdf

5. Conclusions

The spectral and electrical characterization of solar devices is a powerful tool for the development and assessment of solar cells and manufacturing processes. The properties of a solar cell are evaluated by means of the I-V characteristic, from which parameters such as the cell's maximum power output, short circuit current, and open-circuit voltage, in particular, are identified. Additional cell parameters are also required to fully characterize a solar cell, which includes spectral response, fill factor, series resistance, temperature coefficients, and quantum efficiency [25].

This work has focused on the experimental determination of the spectral response and the I-V curves of photovoltaic cells. With this purpose, I used a spectral response equipment located in ITER and another device designed in the optics laboratory of ULL. The calibration of both equipments was verified by means of a mono-crystalline silicon reference cell and the operation of the equipment designed at the ULL can be confirmed. Additionally, outcomes obtained demonstrate the feasibility of the reference cell method reported in the literature [19].

A solar simulator AM 1.5 G was built and an electrometer was calibrated for the measurement of I-V curves. It was possible to simulate the curves at SRC (Standard Reporting Conditions) from experimental data and results were obtained with very good approximation to the data of the manufacturer in different photovoltaic cells. With this, a method for modifying the single-diode parameters of photovoltaic cells and modules to cater for varying conditions of insolation was achieved.

This work lays the foundations of a practical guide for future teaching and research practices, although more studies should be conducted to go deeper this topic. Some of the possible future projections are:

- Study of the influence of the series resistance with the irradiance on the Voc in particular and the I-V characteristic in general.
- Development of a more accurate method to cater for the effects of modules on the I-V characteristics.
- Expansion of the incidence area of illumination and increase of the radiant power of the solar simulator that will allow the characterization of PV modules.
- Study of the efficiency in the infrared spectral range by means of converting materials.
- Influence with the temperature of the efficiency and the electrical characteristics in different solar cells

Acknowledgements

This project has been possible thanks to the Instituto Tecnológico y de Energías Renovables (ITER) and the University of La Laguna (ULL). I am especially grateful to the whole group who form part of the Photovoltaic Laboratory of ITER, for their help, unconditional support and the great interest shown in carrying out this work. My sincere thanks goes to Luis Ocaña and Carlos González Montesdeoca, who provided me with the opportunity to join their team and gave access to the laboratory and research facilities.

Finally, I would like to give special thanks to Dr. Cecilio Hernández Rodríguez, who instructed this project, for his guidance since the beginning, his support and optimism. Without his passionate participation and input, this research could not have been successfully conducted.

6. References

1. Método para calcular la eficiencia cuántica y la respuesta espectral de celdas solares usando LabVIEW. A. J. Aristizábal Cardona. Revista Elementos, 5 (2015).
2. Handbook of Photovoltaic Science and Engineering. Chapter 3: The Physics of the Solar Cell. J. L. Gray. Edited by A. Luque and S. Hegedus. John Wiley & Sons, 2003.
3. Basic Photovoltaic Principles and Methods. Solar Energy Research Institute. USA, 1981.
4. Physics of Solar Energy. Chapter 8: Semiconductor junctions. C. Julian Chen. John Wiley & Sons, 2011.
5. Understanding the p-n junction. A. Sproul. Key Centre for Photovoltaic Engineering, UNSW.
6. Caracterización espectral de células solares comerciales. R. E. Rojas Hernández. Universidad de Salamanca, 2011.
7. Third generation photovoltaics. G. Conibeer. Materials Today, Vol. 10, No. 11, 2007.
8. Third generation photovoltaics: solar cells for 2020 and beyond. M. A. Green. Physica E, 14; 65-70, 2002.
9. Electricidad Solar Fotovoltaica. Vol. II Radiación Solar y Dispositivos Fotovoltaicos. E. Lorenzo. Progensa. Sevilla 2006.
10. Absorption of solar radiation by the atmosphere as determined using satellite, aircraft, and surface data during theAtmospheric Radiation Measurement Enhanced Shortwave Experiment (ARESE). Valero. Journal Of Geophysical Research, 105, 2000.
11. Solar Cells Operating Principles. Technology and System Applications. M.A. Green. University of New South Wales, Australia, 1996.
12. ASTM International, ASTM G173-03 Reference Spectra Derived from SMARTS v.2.9.2. USA 2003.
13. International Renewable Energy Agency, "Solar Photovoltaics", Abu Dhabi, UAE, 2012.
14. A study on Spectral Response and External Quantum Efficiency of Mono-Crystalline Silicon Solar Cell. S. Chander, A. Purohit, A. Nehra, S.P. Nehra and M. S. Dhaka. International Journal of Rnewable Energy Research, Vol. 5, No.1, 2015.
15. Freely available OPV – The fast way to progress. F. C. Krebs, M. Hçsel, M. Corazza, B. Roth, M. V. Madsen, S. A. Gevorgyan, R. R. Søndergaard, D. Karg and M. Jørgensen. Energy Technology, 1; 378-381, 2013.
16. Spectral Characterization of Photovoltaic Devices. Technical Note. Bentham Instruments Ltd.
17. Energy Efficiency Constraints in Photovoltaic Power Generation Systems. S. M. Ferdous, M. A. M. Oninda, Md. H. Maruf, Md. A. Islam and Md. F. Rahman. Journal of Research in Engineering and Applied Sciences, Vol. 3, Issue 02, 2018.
18. External Quantum Efficiency Measurement of solar cell. W. Ananda. 15th Intl. Conf (2017).
19. Calibration of Solar Cells by the Reference Cell Method. C.H. Seaman. Solar Energy, Vol. 29. 291-298. 1982.
20. PVE300 Photovoltaic Device Characterization System. User Manual. Bentham Instrument Limited.
21. Reflections and Refractions in Ray Tracing. B. De Greve, 2006.
22. Color Science: Concepts and methods, quantitative data and formulae. G. Wyszecki and W. S. Stiles. 2nd Edition. John Wiley & Sons. New York, 1982
23. Methods of Soil Analysis. Part 5. Mineralogical Methods. Chapter 13: Diffuse Reflectance Spectroscopy. J. Torrent and V. Barrón. Edited by Soil Science Society of America, 2008.
24. Variations of PV module parameters with irradiance and temperature. Haider Ibrahim and Nader Anani. Energy Procedia 134, 276-285 (2017)
25. Solar cell characterization. Behrang H. Hamadani and Brian Dougherty.

Annexes

A.1. Quantum efficiency of an ideal solar cell and of a standard silicon solar cell accounting for the different recombination mechanisms [15]

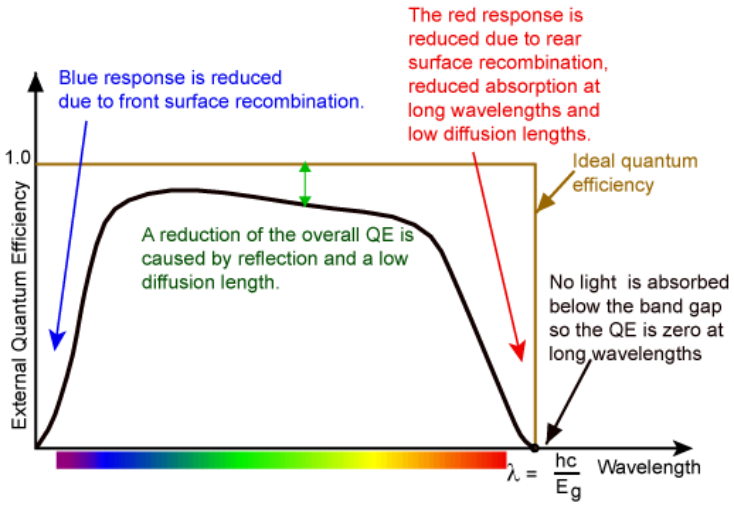

A.2. Generic I-V curve of a solar cell under illumination [(1)]

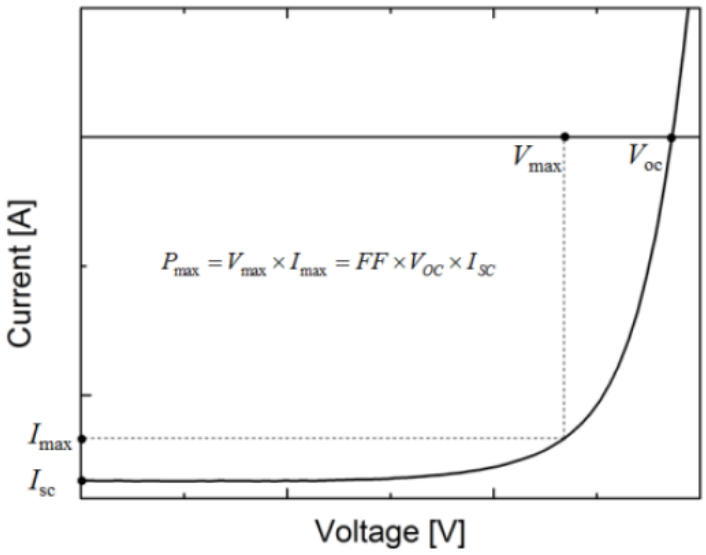

(1) Solar cell characterization. Behrang H. Hamadani and Brian Dougherty.

A.3. EQE measurement equipment employed at the ULL Optics Laboratory

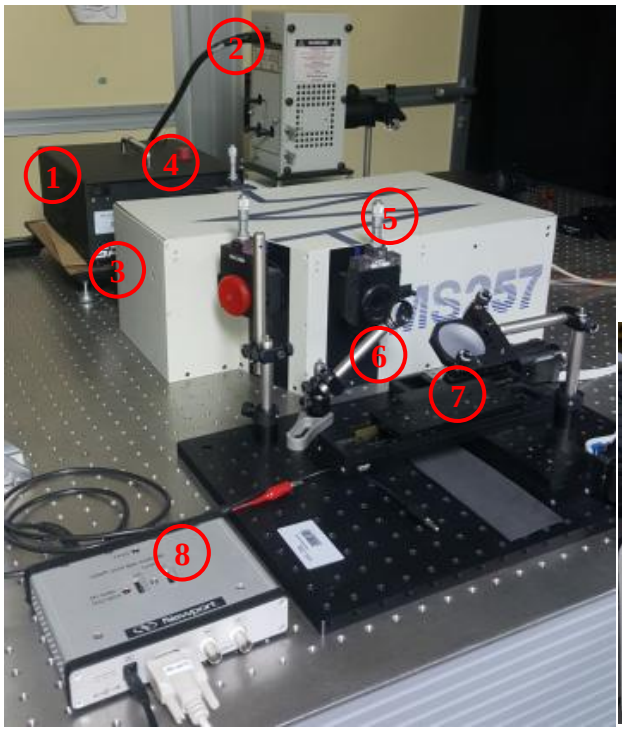

(1) W lamp
(2) Xe lamp
(3) MS257 Monochromator
(4) Entrance slit
(5) Exit slit
(6) Lens
(7) Mirror
(8) Lock-in amplifier
(9) Chopper

A.4. Bentham PVE300 Photovoltaic device characterization system [18]

A.5. Components of a solar simulator [(2)]

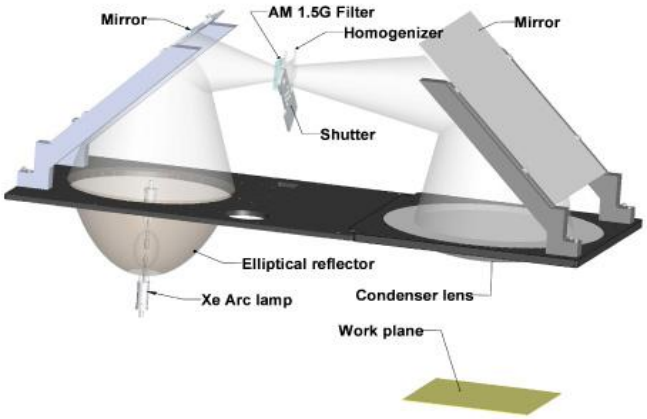

(2) http://abet-technologies.com/solar-simulators/solar-simulator-elements/

A.6. Connections for the I-V measurement of a device under test (DUT) [(3)]

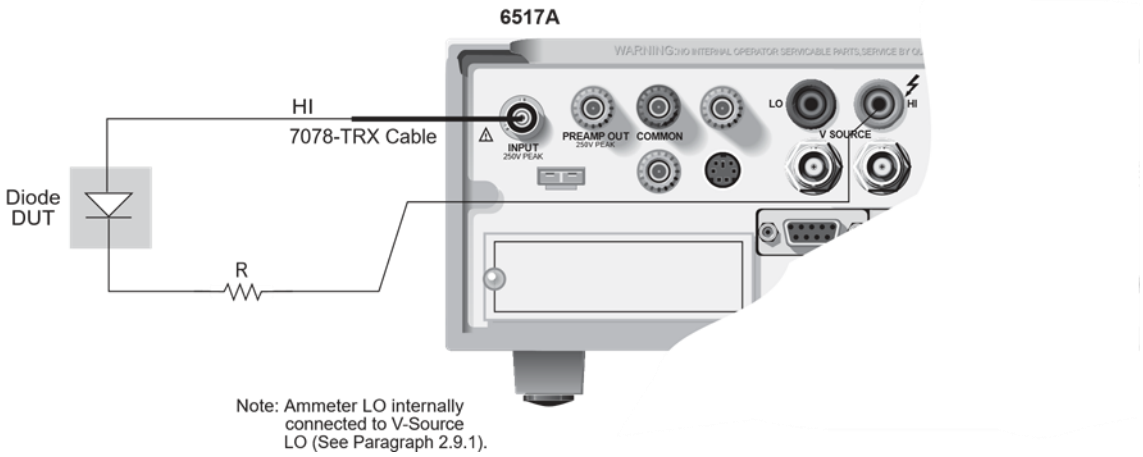

(3) Model 6517A Electrometer User´s Manual, 1996 Keithley Instruments, Inc.

A.7. I-V measurement system employed at the ULL Optics Laboratory

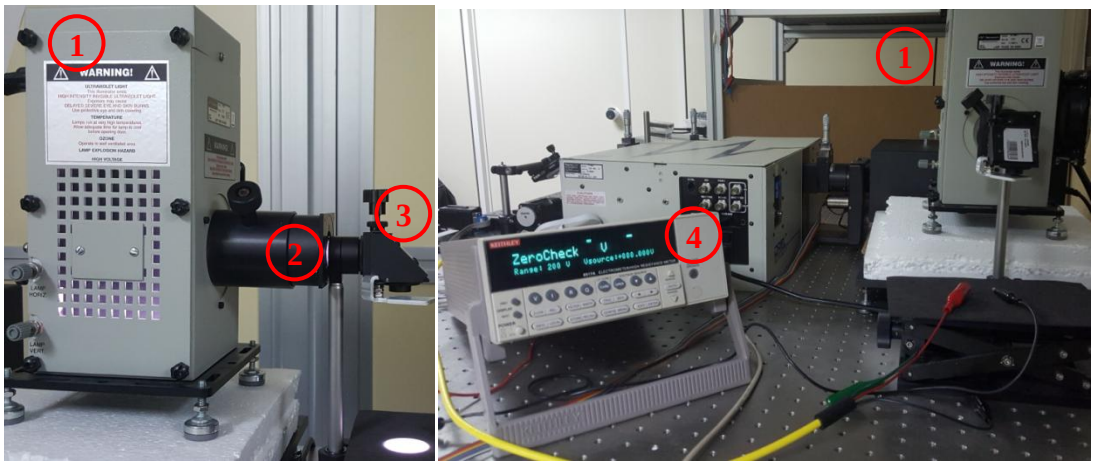

(1) Newport 67001 Xe lamp from Oriel
(2) AM1.5G solar filter
(3) Lenses + Mirror
(4) Keithley 6517A Electrometer

A.8. Equivalent circuit for I-V measurement